A Conservative a-Posteriori Time-Limiting Procedure in Quinpi Schemes

A conservative a-posteriori time-limiting procedure in Quinpi schemes

Giuseppe Visconti, Silvia Tozza, Matteo Semplice and Gabriella Puppo

Abstract The superior stability properties of implicit time schemes allow to avoid small time steps required to satisfy restrictive stability conditions for stiff hyperbolic systems. In (Puppo et al., Comm. Appl. Math. & Comput., 2022) an implicit third order finite volume scheme based on a third order DIRK combined with a third order CWENO reconstruction for the space-limiting was proposed. The originality of the proposed method, named Quinpi, lies in the computation of a first order implicit predictor which is used to fix the nonlinear weights of the space reconstruction, thus simplifying considerably the non-linearity of the scheme. However, the time-limiting in the above mentioned paper, which is necessary to control spurious oscillations in the implicit time integration, requires a conservative correction. In this work, we address this problem and we propose a conservative a-posteriori time-limiting procedure inspired by the MOOD method. The numerical experiments show the reliability of the proposed scheme and include both linear and nonlinear scalar conservation laws.

Keywords. Conservation laws; High-order schemes; Time-limiting; Implicit methods; CWENO reconstruction.

Giuseppe Visconti
Department of Mathematics, Sapienza University of Rome, P.le Aldo Moro 5, 00185 Rome (Italy). e-mail: giuseppe.visconti@uniroma1.it

Silvia Tozza
Department of Mathematics, University of Bologna, Piazza di Porta S. Donato 5, 40126 Bologna (Italy). e-mail: silvia.tozza@unibo.it

Matteo Semplice
Dipartimento di Scienza e Alta Tecnologia, Università degli Studi dell'Insubria, Via Valleggio 11, 22100 Como (Italy). e-mail: matteo.semplice@uninsubria.it

Gabriella Puppo
Deptartment of Mathematics, Sapienza University of Rome, P.le Aldo Moro 5, 00185 Rome (Italy). e-mail: gabriella.puppo@uniroma1.it

1 Introduction

Many interesting propagation phenomena can be described by systems of one-dimensional partial differential equations (PDEs) of the form

$$\partial_t u(x,t) + \partial_x f(u(x,t)) = 0, \tag{1}$$

where $u : \mathbb{R} \times [0, +\infty) \to \mathbb{R}^m, m \geq 1$, is the unknown solution, and $f : \mathbb{R}^m \to \mathbb{R}^m$ is the vector of the flux functions. System (1) is said *hyperbolic* if the eigenvalues $\{\lambda_j(u)\}_{j=1}^m$ of the Jacobian of f are real, i.e. the propagation speeds of the waves are finite, and there exists a complete set of eigenvectors. In addition, system (1) is said *stiff* if $\frac{\max_{j=1,\dots,m} |\lambda_j(u)|}{\min_{j=1,\dots,m} |\lambda_j(u)|} \gg 1$, namely if the solution u is characterized by waves with very different speeds. This case is relevant in many physical applications, such as Low-Mach problems in gas dynamics, kinetic problems close to equilibrium.

The stiffness of the system introduces numerical difficulties when using explicit schemes which require a very small time step to meet the restrictive Courant-Friedrichs-Levy (CFL) stability condition. A huge literature has been developed for the numerical treatment of these problems. Here we refer to the non-exhaustive list [1, 6, 16–18, 33] for Low-Mach problems and to [19, 26, 29] for kinetic equations.

We will focus on the high-order implicit finite volume numerical approximation of stiff hyperbolic equations, specifically on the recent work [30] where a third order implicit scheme for scalar conservation laws was proposed. The numerical scheme in [30] was named Quinpi. The third order accuracy was achieved by using a third order Diagonally Implicit Runge-Kutta (DIRK) for the time integration and a third order Central Weighted Essentially Non Oscillatory (CWENO) reconstruction, cf. [14], for the space discretization. However, the use of CWENO to perform space-limiting, necessary to prevent spurious oscillations typical of high order schemes, introduces a source of non-linearity which becomes computationally challenging in the implicit time integration. The novel idea of [30] is to simplify considerably the non-linearity of the space-limiting procedure through the computation of a first order implicit predictor, which is used to freeze the nonlinear weights of the CWENO reconstruction. This approach makes the Quinpi scheme linear on linear problems. Instead, on nonlinear problems the only source of non-linearity is due to the nonlinear flux function, which is in turn due to the physical structure of the model, and therefore is unavoidable. The first order implicit scheme is based on a composite backward Euler, which is evaluated at the abscissae of the DIRK, naturally combined with a piecewise constant (i.e. non-limited) reconstruction in space. As noted in [4, 30], the space-limiting is not sufficient to control the appearance of spurious oscillations in implicit integration, especially for large Courant numbers. A time-limiting procedure is required, which is achieved by a nonlinear blending of the first order predictor and of the third order solution at each time level. In particular, in [30] the blending of the cell averages of the two solutions is performed in a CWENO framework using a combination of space and time regularity indicators.

Similar approaches to the Quinpi schemes have been developed in the literature. We mention, for instance, the fifth order implicit Weighted Essentially Non Oscil-

latory (WENO) schemes in [24], where a predictor-corrector technique is also used. The predictor used in [24] is based on an explicit first order scheme and therefore it does not allow to use large time steps. A fully nonlinear implicit scheme, based on a third order RADAU time integrator and a third order WENO reconstruction, which is limited in both space and time simultaneously, can be found in [4]. Fully implicit, semi-implicit, implicit-explicit and local time-stepping treatments of stiff hyperbolic systems have been investigated, e.g., in [5, 10–13, 22, 23].

In this work, we address the problem of the time-limiting in Quinpi schemes. In particular, the nonlinear blending proposed in [30] has the drawback of being non-conservative and, thus, of requiring a conservative correction at each time step. Here, we propose a different approach to control the spurious oscillations through a conservative a-posteriori time-limiting procedure which draws inspiration from the Multi-dimensional Optimal Order Detection (MOOD) method introduced in [8, 9] in order to reduce the order of the space reconstruction on problematic cells. A similar idea has been investigated in [21] where a MOOD-inspired technique controls unphysical oscillations of high order implicit numerical solutions of the water flow in district heating networks. MOOD has been also extended to other contexts, as for instance in [28, 31, 34]. Furthermore, in this work we also investigate the use of a first order predictor based on the continuous extension [35] of the backward Euler time integrator.

The chapter is organized as follows: In Section 2 we first review the third order Quinpi algorithm proposed in [30]. Next, we discuss the two modifications which motivate this work, namely the computation of the predictor using the first order continuous extension of backward Euler and the conservative a-posteriori time-limiting. In Section 3 we test the schemes on linear and nonlinear scalar conservation laws, comparing the results with the Quinpi scheme in [30]. Finally, in Section 4 we summarize the contributions of this work and discuss future perspectives.

2 Quinpi scheme for hyperbolic conservation laws

In order to introduce the third order Quinpi scheme, we briefly recall the finite volume setting for the numerical approximation of (1).

We consider a uniform discretization of the compact computational domain $\Omega \subset \mathbb{R}$ made by N cells $\Omega_j = [x_j - h/2, x_j + h/2]$ of amplitude $h > 0$. The computational domain Ω is thus covered by the cells Ω_j in such a way $\cup_j \Omega_j = \Omega$. We define the cell averages of the exact solution on the cells Ω_j as $\overline{u}_j(t) = \frac{1}{h}\int_{\Omega_j} u(x,t)\mathrm{d}x$. Using the method of lines (MOL), conservation law (1) can be written in the semi-discrete form

$$\frac{\mathrm{d}\overline{u}_j(t)}{\mathrm{d}t} = -\frac{1}{h}\left[f\left(u\left(x_j + \tfrac{h}{2}, t\right)\right) - f\left(u\left(x_j - \tfrac{h}{2}, t\right)\right)\right]. \tag{2}$$

Notice that (2) is still exact since it describes the exact evolution of the cell averages as the difference of the fluxes at the cell boundaries.

To transform system (2) in a numerical scheme for the approximation of the cell averages, one has to introduce several ingredients.

Space reconstruction with CWENO.

The solution of system (2), which evolves cell averages, requires the knowledge of point values of the solution at the cell interfaces. The problem of computing these values using the information of the cell averages is called *the reconstruction problem* and can be solved by a reconstruction algorithm $\mathcal{R} : \{\overline{u}_j(t)\} \mapsto \mathcal{R}\left(\{\overline{u}_j(t)\}\right)$. Classical examples are the WENO and CWENO reconstruction procedures, see [14, 25, 27, 32], and their developments, where $\mathcal{R}$ is suitably defined in order to prevent spurious oscillations in space.

In CWENO type reconstructions, the operator $\mathcal{R}$ provides a space limited approximation of the exact solution $u(\cdot, t)$, $t \geq 0$, as $u(x,t) \approx \sum_j R_j(x;t)\chi_{\Omega_j}(x)$, where χ_{Ω_j} is the characteristic function of the cell Ω_j, and $R_j(x;t)$ is the reconstruction polynomial of degree d on $x \in \Omega_j$, which depends on time through the time-dependent cell averages. With the reconstruction algorithm $\mathcal{R}$ we can estimate the values $u\left(x_j \pm {}^{h}/_{2}, t\right)$, $t \geq 0$, from the knowledge of the cell averages only. More precisely, the reconstruction algorithm provides the following values at each cell interface

$$u^{-}_{j+1/2}(t) = R_j\left(x_j + \tfrac{h}{2}; t\right), \quad u^{+}_{j+1/2}(t) = R_{j+1}\left(x_j + \tfrac{h}{2}; t\right), \tag{3}$$

which are named *boundary extrapolated data* (BED). We recall that with CWENO it is possible to reconstruct uniformly accurate and non-oscillatory point values of the solution at any point $x \in \Omega$.

Following [30], we focus on third order CWENO schemes in which the restriction of the operator $\mathcal{R}$ on a cell Ω_j can be defined as

$$\mathcal{R}_{|\Omega_j} : \{\overline{u}_k(t)\}_{k=j-1}^{j+1} \mapsto R_j(x;t) = \omega_{j,0}P_{j,0}(x) + \omega_{j,L}P^{(1)}_{j,L}(x) + \omega_{j,R}P^{(1)}_{j,R}(x).$$

Here, $P^{(1)}_{j,L}$ and $P^{(1)}_{j,R}$ are linear polynomials interpolating $\{\overline{u}_{j-1}(t), \overline{u}_j(t)\}$ and $\{\overline{u}_j(t), \overline{u}_{j+1}(t)\}$, respectively, in the sense of cell averages. Whereas, $P_{j,0}$ is the second degree second order accurate polynomial

$$P_{j,0}(x) = \frac{1}{d_0}\left(P^{(2)}_j(x) - d_L P^{(1)}_{j,L}(x) - d_R P^{(1)}_{j,R}(x)\right)$$

where $d_0, d_L, d_R \in (0,1)$ with $d_0 + d_L + d_R = 1$ are the so-called linear or optimal coefficients, and $P^{(2)}_j(x)$ is the polynomial of degree 2 interpolating $\{\overline{u}_{j-1}(t), \overline{u}_j(t), \overline{u}_{j+1}(t)\}$ in the sense of cell averages. Observe that all these polynomials are time dependent, but we have suppressed the time dependencies for a better readability. For a detailed formulation of all these polynomials we refer the interested reader to [30, Section 3.1]. Finally, $\omega_{j,0}, \omega_{j,L}, \omega_{j,R} \in (0,1)$ are the nonlinear

weights which depend non-linearly on the cell averages. They are suitably defined, with the help of nonlinear regularity indicators, such as the Jiang-Shu smoothness indicators [25], in order to select the highest order of accuracy of the reconstruction on smooth flows and to downgrade to lower order non-oscillatory reconstructions on discontinuous solutions. Although several definitions of the nonlinear weights have been studied in the literature [2, 7, 15], we use the classical WENO type definition as in [30].

Notice that, in principle, the two BED in (3) obtained with the reconstruction algorithm are different, although computed at the same interface $x_{j+h/2}$, with $\left|u^+_{j+1/2}(t) - u^-_{j+1/2}(t)\right| = O(h^{d+1})$ on smooth flows. Therefore, in order to approximate the flux function at the interfaces, one introduces a consistent and monotone numerical flux $\mathcal{F}(a,b)$ such that $f(u(x_{j+1/2},t)) \approx \mathcal{F}_{j+1/2}(t) = \mathcal{F}(u^-_{j+1/2}(t), u^+_{j+1/2}(t))$. The function $\mathcal{F}$ may be any approximate or exact Riemann solver. Finally, one obtains the system of ordinary differential equations (ODEs)

$$\frac{\mathrm{d}\overline{u}_j(t)}{\mathrm{d}t} = -\frac{1}{h}\left[\mathcal{F}_{j+\frac{1}{2}}(t) - \mathcal{F}_{j-\frac{1}{2}}(t)\right], \tag{4}$$

which provides the approximation of the PDE solution. From now on, we omit the dependence on t in order to lighten the notation.

Time integration with DIRK.

The semi-discrete approach with the MOL completely defines the system of ODEs (4). It is worth to notice that now $\overline{u}_j$ is an approximation of the exact cell average on Ω_j. In order to obtain a fully discrete scheme, one needs to approximate (4) with a time integration scheme. If we focus on Runge-Kutta (RK) schemes with s stages and general Butcher tableau

$$\begin{array}{c|cccc} c_1 & a_{11} & a_{12} & \dots & a_{1s} \\ c_2 & a_{21} & a_{22} & \dots & a_{2s} \\ \vdots & \vdots & \vdots & \ddots & \\ c_s & a_{s1} & a_{s2} & \dots & a_{ss} \\ \hline & b_1 & b_2 & \dots & b_s \end{array} \tag{5}$$

the time discretization of (4) leads to

$$\begin{aligned} \overline{u}_j^{n+1} &= \overline{u}_j^n - \frac{\Delta t}{h} \sum_{k=1}^{s} b_k \left[\mathcal{F}^{(k)}_{j+\frac{1}{2}} - \mathcal{F}^{(k)}_{j-\frac{1}{2}} \right], \quad n \geq 0, \ \forall\, j, \\ \mathcal{F}^{(k)}_{j+\frac{1}{2}} &= \mathcal{F}\left(u^{-,(k)}_{j+\frac{1}{2}}, u^{+,(k)}_{j+\frac{1}{2}} \right) \end{aligned} \tag{6}$$

where Δt is the time step, and now $\overline{u}_j^n$ denotes an approximation of the exact cell average at time $n\Delta t$, namely $\frac{1}{h}\int_{\Omega_j} u(x, n\Delta t)\mathrm{d}x$. Finally, $u^{\mp,(k)}_{j\pm 1/2}$ are BED from the stage values

$$\overline{u}_j^{(k)} = \overline{u}_j^n - \frac{\Delta t}{h} \sum_{\ell=1}^{s} a_{k\ell} \left[\mathcal{F}^{(\ell)}_{j+\frac{1}{2}} - \mathcal{F}^{(\ell)}_{j-\frac{1}{2}} \right], \quad \ell = 1, \ldots, s, \tag{7}$$

approximations of the solution at times $t^{(k)} = (n + c_k)\Delta t$. Typical assumption is that $c_k = \sum_{\ell=1}^{s} a_{k\ell}$, $k = 1, \ldots, s$, and one has $\sum_{k=1}^{s} b_k = 1$ for consistency. Clearly, one uses RK schemes with order matching the order of the space approximation.

It is well known that for explicit schemes, in the case of RK when $a_{k\ell} = 0$, $\ell \geq k$, the time step Δt must satisfy the CFL stability condition $\lambda := \Delta t/h \leq 1/\max_{i=1,\ldots,m} |\lambda_i(u)|$. We recall that the $\lambda_i(u)$ are the eigenvalues of the Jacobian of the flux function f, namely the propagation speeds of the waves. Thus, if the system is stiff, i.e. characterized by fast waves, the CFL condition becomes very restrictive imposing the use of a very small time step for stability problems and not for accuracy. A way to overcome this restriction is to build implicit schemes with unconditional stability, e.g. based on DIRK schemes, for which $a_{k\ell} = 0$, $\ell > k$. The advantage of DIRK schemes is that the implicit computation of a given stage value (7) is independent from the following ones. Therefore, for each time step one has to solve the s nonlinear systems of equations

$$G_j\left(\overline{u}^{(k)}\right) := \overline{u}_j^{(k)} + \frac{a_{kk}\Delta t}{h} \left[\mathcal{F}^{(k)}_{j+\frac{1}{2}} - \mathcal{F}^{(k)}_{j-\frac{1}{2}} \right] - \overline{u}_j^n + \frac{\Delta t}{h} \sum_{\ell=1}^{k-1} a_{k\ell} \left[\mathcal{F}^{(\ell)}_{j+\frac{1}{2}} - \mathcal{F}^{(\ell)}_{j-\frac{1}{2}} \right] = 0.$$

We have highlighted the difference of the k-th numerical fluxes to emphasize that this makes the system $G(u) = 0$ nonlinear. In fact, G has two sources of non-linearity:

1. From the physics, if the phenomenon under study is described by a nonlinear flux function f in (1), and cannot be avoided;
2. Due to the high-order space discretization, since the numerical fluxes $\mathcal{F}^{(k)}_{j\pm 1/2}$ are computed on the BED of $\overline{u}_j^{(k)}$, obtained by the reconstruction procedure, which is nonlinear through the nonlinear weights even for linear problems. Therefore, even for linear PDEs, the implicit scheme requires a nonlinear solver to find the solution of $G(u) = 0$. This results in a prohibitive computational cost.

The Quinpi approach provides a way to circumvent the non-linearity determined by the high-order reconstruction procedure as described in the next subsection.

2.1 The Quinpi approach

The Quinpi idea [30] is explained in the case of scalar conservation laws, i.e. taking $m = 1$ in (1). The name Quinpi stands for implicit CWENO and it is based on a predictor-corrector approach to tackle the second source of non-linearity discussed previously. To this end, an approximation of the solution at the s intermediate times $t^{(k)} \in [n\Delta t, (n+1)\Delta t]$, $k = 1, \dots, s$, defined by the abscissae of the DIRK method is computed with a linear implicit low order scheme. The predictor solutions are then used to avoid the non-linearities of the high order method, the corrector, which are induced by the reconstruction procedure. In fact, it is possible to write the BED (3) at stage k as

$$u^{-,(k)}_{j+\frac{1}{2}} = \sum_{\ell=-1}^{1} W_{j,\ell}\left(x_{j+1/2}\right) \overline{u}^{(k)}_{j+\ell}, \quad u^{+,(k)}_{j+\frac{1}{2}} = \sum_{\ell=-1}^{1} W_{j+1,\ell}\left(x_{j+1/2}\right) \overline{u}^{(k)}_{j+1+\ell}, \tag{8}$$

where the weights $\{W_{j,\ell}(\cdot), W_{j+1,\ell}(\cdot)\}_{\ell=-1,0,1}$ contain the nonlinear part of the reconstruction. Then, if these weights are computed on the predictor scheme, they become constant with respect to the cell averages $\overline{u}^k$. In this way, the complete scheme is linear with respect to the space reconstruction in the sense that the solution of $G(u) = 0$ is obtained by solving sequentially s systems which are nonlinear only through the flux function f.

2.1.1 The predictor: Composite backward Euler vs continuous extension

In order to obtain a predictor of the solution, we approximate system (2) with an implicit first order scheme. Specifically, in [30] the composite backward Euler method is employed providing s approximations, say $\overline{u}^{\mathsf{BE},(k)}$, $k = 1, \dots, s$, within the time step $[n\Delta t, (n+1)\Delta t]$ of the high order scheme. Without loss of generality, assume that the abscissae of the DIRK method are ordered. Then, the k-th first order solution $\overline{u}^{\mathsf{BE},(k)}$ advances the solution from $t^{(k-1)} = (n+c_{k-1})\Delta t$ to $t^{(k)} = (n+c_k)\Delta t$, with the notation convention $c_0 = 0$. Overall, one has

$$\begin{aligned}
\overline{u}^{\mathsf{BE},n+1}_j &= \overline{u}^n_j - \frac{\Delta t}{h} \sum_{k=1}^{s} \theta_k \left[\mathcal{F}^{\mathsf{BE},(k)}_{j+\frac{1}{2}} - \mathcal{F}^{\mathsf{BE},(k)}_{j-\frac{1}{2}} \right], \quad n \geq 0, \ \forall\, j, \\
\mathcal{F}^{\mathsf{BE},(k)}_{j+\frac{1}{2}} &= \mathcal{F}\left(\overline{u}^{\mathsf{BE},(k)}_j, \overline{u}^{\mathsf{BE},(k)}_{j+1} \right) \\
\overline{u}^{\mathsf{BE},(k)}_j &= \overline{u}^{\mathsf{BE},(k-1)}_j - \frac{\theta_k \Delta t}{h} \left[\mathcal{F}^{\mathsf{BE},(k)}_{j+\frac{1}{2}} - \mathcal{F}^{\mathsf{BE},(k)}_{j-\frac{1}{2}} \right], \quad k = 1, \dots, s,
\end{aligned} \tag{9}$$

where $\theta_k := c_k - c_{k-1}$ and $\overline{u}^{\mathsf{BE},(0)}_j := \overline{u}^n_j$.

Notice that the numerical flux function $\mathcal{F}$ in (9) is now computed on piecewise constant reconstructions from the cell averages. In fact, first order predictors do

not require space-limiting, because they are unconditionally Total Variation Diminishing. Therefore, despite of the high order scheme, the first order predictor (9) is characterized by a single non-linearity, that is the one induced by the flux function f, which requires to solve the nonlinear system

$$G_j(\overline{u}^{\mathsf{BE},(k)}) := \overline{u}_j^{\mathsf{BE},(k)} + \frac{\theta_k \Delta t}{h}\left[\mathcal{F}_{j+\frac{1}{2}}^{\mathsf{BE},(k)} - \mathcal{F}_{j-\frac{1}{2}}^{\mathsf{BE},(k)}\right] - \overline{u}_j^{\mathsf{BE},(k-1)} = 0 \tag{10}$$

at each stage.

However, the solution of (10) requires the use of a numerical method, such as the Newton's method, s times within a single time step and this may be computationally expensive. In this work we explore a way to reduce this complexity which relies on the continuous extensions of RK schemes [35]. More precisely, we compute the predictor solution only at time $(n+1)\Delta t$ solving one nonlinear system in each time step. Then, we recover the first order approximations at the times $t^{(k)} = [n\Delta t, (n+1)\Delta t]$ as linear interpolation between $\overline{u}_j^n$ and $\overline{u}_j^{\mathsf{BE},n+1}$. Overall, we have

$$\begin{aligned}
\overline{u}_j^{\mathsf{BE},n+1} &= \overline{u}_j^n - \frac{\Delta t}{h}\left[\mathcal{F}_{j+\frac{1}{2}}^{\mathsf{BE},n+1} - \mathcal{F}_{j-\frac{1}{2}}^{\mathsf{BE},n+1}\right], \quad n \geq 0, \ \forall\, j, \\
\mathcal{F}_{j+\frac{1}{2}}^{\mathsf{BE},n+1} &= \mathcal{F}\left(\overline{u}_j^{\mathsf{BE},n+1}, \overline{u}_{j+1}^{\mathsf{BE},n+1}\right) \\
\overline{u}_j^{\mathsf{BE},(k)} &= \overline{u}_j^n - \frac{c_k \Delta t}{h}\left[\mathcal{F}_{j+\frac{1}{2}}^{\mathsf{BE},n+1} - \mathcal{F}_{j-\frac{1}{2}}^{\mathsf{BE},n+1}\right], \quad k = 1, \ldots, s.
\end{aligned} \tag{11}$$

This approach has the advantage to re-use the numerical fluxes at time level $(n+1)\Delta t$ to compute the $\overline{u}_j^{\mathsf{BE},(k)}$, and thus it results in a lower computational cost compared to (9).

Once the first order predictions are obtained, either with (9) or by (11), they are used to evaluate the nonlinear terms $\{W_{j,\ell}(\cdot), W_{j+1,\ell}(\cdot)\}_{\ell=-1,0,1}$ of the high order BED (8). Finally, from (6)-(7) one obtains the high order solution $\overline{u}_j^{n+1}$ at time level $(n+1)\Delta t$.

2.1.2 A conservative a-posteriori time-limiting

The Quinpi scheme ends with the limiting of the high order solution. In fact, when using a large Δt, the space limiting is not enough to prevent the spurious oscillations of high order schemes. In this case, as noticed in [4, 20, 30], limiting in time is also required. In particular, in [30] the time limiting is performed in a CWENO-like framework. There, the limiting is applied on the computed high order solution, blending it with the low order predictor which is a reliable, stable and non-oscillatory solution. However, the procedure in [30] does not have mass conservation property and must be followed up by a suitable conservative correction.

Here, we address this issue and propose a conservative a-posteriori time-limiting inspired by the MOOD technique proposed by Diot, Clain and Loubère in [8, 9]. MOOD is originally designed as an a-posteriori space-limiting technique for multi-dimensional finite volume schemes. Instead, we use the typical MOOD detectors to limit the high order solution of the Quinpi approach at time level $(n+1)\Delta t$. Specifically, on the cells where the MOOD criteria detect an oscillatory behavior, we replace the fluxes at the cell interfaces with a convex combination of the high order and the low order numerical fluxes. We point out that a similar idea has been investigated in [21], where an a-posteriori limiting for fully implicit finite volume schemes on transport networks is proposed.

Whenever the a-posteriori limiting finds that Ω_ℓ is a problematic cell, for some $\ell \in \{1, \dots, N\}$, the high order numerical fluxes $\mathcal{F}^{(k)}_{\ell\pm1/2}$ are replaced by the limited fluxes

$$\mathcal{F}^{\mathsf{TL},(k)}_{\ell\pm1/2} = (1-\alpha_{\mathsf{TL}})\theta_k \mathcal{F}^{\mathsf{BE},(k)}_{\ell\pm1/2} + \alpha_{\mathsf{TL}} b_k \mathcal{F}^{(k)}_{\ell\pm1/2}, \quad \alpha_{\mathsf{TL}} \in [0,1], \tag{12}$$

where the acronym TL stands for Time-Limited. Of course, if neither Ω_ℓ nor $\Omega_{\ell+1}$ are problematic, $\mathcal{F}^{\mathsf{TL},(k)}_{\ell+1/2} = b_k \mathcal{F}^{(k)}_{\ell+1/2}$. Thus, the high order numerical fluxes at the interfaces of the problematic cell Ω_ℓ are blended with the low order numerical fluxes reducing locally the order of the solution recomputing

$$\overline{u}_j^{n+1} = \overline{u}_j^n - \frac{\Delta t}{h} \sum_{k=1}^{s} \left[\mathcal{F}^{\mathsf{TL},(k)}_{j+\frac{1}{2}} - \mathcal{F}^{\mathsf{TL},(k)}_{j-\frac{1}{2}} \right], \quad j = \ell-1, \ell, \ell+1. \tag{13}$$

The time-limited fluxes are computed as in (12) when the predictor is obtained with the composite backward Euler, which provides all the low order numerical fluxes $\mathcal{F}^{\mathsf{BE},(k)}_{\ell\pm1/2}$, $k = 1, \dots, s$. Instead, when the predictor is computed with the use of the continuous extension, the high order numerical fluxes $\mathcal{F}^{(k)}_{\ell\pm1/2}$ are replaced by

$$\mathcal{F}^{\mathsf{TL},(k)}_{\ell\pm1/2} = \frac{1}{s} \mathcal{F}^{\mathsf{BE},n+1}_{\ell\pm1/2}. \tag{14}$$

In order to determine where the time limiting has to occur, we detect spurious oscillations using the following criteria, inspired by the ones proposed in [9].

Extrema Detector (ED). The ED criterion checks if a cell Ω_j has a local extremum of the solution at time $(n+1)\Delta t$, i.e. if $\overline{u}_j^{n+1}$ satisfies

$$h^2 < \min\left\{\overline{u}_{j-1}^{n+1}, \overline{u}_{j+1}^{n+1}\right\} - \overline{u}_j^{n+1} \quad \text{or} \quad h^2 < \overline{u}_j^{n+1} - \max\left\{\overline{u}_{j-1}^{n+1}, \overline{u}_{j+1}^{n+1}\right\}.$$

If Ω_j does not have an extremum, then the approximation $\overline{u}_j^{n+1}$ is assumed to be valid. Otherwise, one has to determine if $\overline{u}_j^{n+1}$ is a physical extremum or a spurious oscillation, determined either by the high order scheme or by floating point errors.

Let us define a fourth order approximation of the second derivative of the solution in x_j at time $t^{n+1} = (n+1)\Delta t$ from cell averages as

$$\frac{\mathrm{d}^2 u(x,t^{n+1})}{\mathrm{d}x^2}|_{x=x_j} \approx C_j := \frac{-\overline{u}_{j-2}^{n+1} + 12\overline{u}_{j-1}^{n+1} - 22\overline{u}_j^{n+1} + 12\overline{u}_{j+1}^{n+1} - \overline{u}_{j+2}^{n+1}}{8h^2}.$$

Then, C_j provides a discrete approximation of the local curvature in Ω_j and based on the following indicators

$$\chi_{j,m} := \min\left\{C_{j-1}, C_j, C_{j+1}\right\}, \quad \chi_{j,M} := \max\left\{C_{j-1}, C_j, C_{j+1}\right\}$$

one distinguishes the type of the extremum with the subsequent criteria.

Plateau Detector (PD). If the total curvature $\max\left\{|\chi_{j,m}|, |\chi_{j,M}|\right\}$ is close to zero, then the found extremum in Ω_j is an artifact due to round off errors and the solution $\overline{u}_j^{n+1}$ is considered valid. The presence of the local plateau is numerically checked thanks to the following condition

$$\max\left\{|\chi_{j,m}|, |\chi_{j,M}|\right\} < h.$$

Instead, if Ω_j does not have a local plateau, then one investigates the nature of the extremum with the following criteria.

Local Oscillation Detector (LOD). A spurious oscillation occurs in Ω_j if the sign of the curvature changes, i.e., if one observes numerically

$$\chi_{j,m}\chi_{j,M} < 10^{-8}.$$

If a local oscillation is found, then the time-limiting occurs as in (12) or (14). Otherwise, one checks if the extremum is smooth with the following detector.

Smoothness Detector (SD). There is a smooth extremum if

$$\frac{1}{4} < \frac{\min\left\{|\chi_{j,m}|, |\chi_{j,M}|\right\}}{\max\left\{|\chi_{j,m}|, |\chi_{j,M}|\right\}} < 1.$$

If the extremum is not smooth, then the time-limiting occurs as in (12) or (14).

In the numerical experiments of this chapter we consider only linear transport and Burgers equations, for which the admissible states are the entire $\mathbb{R}$ and the computer code does not perform operations that could lead to the occurrence of NaN values in the numerical solutions. Thus, contrary to classical MOOD detectors, we do not use the Physical Admissibility Detection (PAD) criterion [8], which checks if the solution stays in physically meaningful regimes.

What makes the present time-limiting approach conservative is the blending of the numerical fluxes instead of the blending of the solutions as done in [30]. The parameter α_{TL} in (12) is problem dependent, since it depends on the type of equation, presence of stiffness, initial profile chosen, etc.

3 Numerical Tests

In this section, we consider standard tests which are commonly used in the literature on high-order methods for scalar conservation laws: linear advection of non-smooth waves, shock formation and interaction in the nonlinear Burgers equation.

All the numerical simulations are performed with the third order Quinpi scheme in [30] named Q3P1 and with the Quinpi schemes of this work based on the conservative a-posteriori time-limiting inspired by MOOD. In particular, we name $\mathsf{Q3P1}_{\mathsf{MOOD}}$ the third order scheme with the composite backward Euler as predictor and $\mathsf{Q3P1}_{\mathsf{CEMOOD}}$ the third order scheme where the predictor is computed with the continuous extension.

All the schemes are built using the third order CWENO reconstruction with the optimal coefficients $d_0 = 3/4$, $d_L = d_R = 1/8$, whereas the nonlinear weights $w_{j,k}$, $k = 0, L, R$, $\forall\, j$, are computed using the Jiang-Shu regularity indicators, see [25], with parameter $\epsilon = h^2$. For the purposes of this work it is sufficient to consider the Lax-Friedrichs numerical flux

$$\mathcal{F}(u^-, u^+) = \frac{1}{2}\left(f(u^+) + f(u^-) - \alpha(u^+ - u^-)\right), \tag{15}$$

with $\alpha = \max_u |f'(u)|$. The time integrator is the three stage third order L-stable DIRK scheme of [3] with Butcher tableau

$$\begin{array}{c|ccc} \lambda & \lambda & 0 & 0 \\ \frac{(1+\lambda)}{2} & \frac{(1-\lambda)}{2} & \lambda & 0 \\ 1 & -\frac{3}{2}\lambda^2 + 4\lambda - \frac{1}{4} & \frac{3}{2}\lambda^2 - 5\lambda + \frac{5}{4} & \lambda \\ \hline & -\frac{3}{2}\lambda^2 + 4\lambda - \frac{1}{4} & \frac{3}{2}\lambda^2 - 5\lambda + \frac{5}{4} & \lambda \end{array} \tag{16}$$

where $\lambda = 0.4358665215$. The Courant numbers (Cou) and the values α_{TL} of the conservative a-posteriori time-limiting are specified in each numerical test.

3.1 Test 1: Experimental order of convergence

First of all, we study the accuracy of the Quinpi scheme proposed in this work by numerically computing the rate of convergence. Similarly to what was done in [4,30], we consider the nonlinear Burgers equation, that is

$$\partial_t u(x,t) + \partial_x\left(\frac{u^2(x,t)}{2}\right) = 0, \tag{17}$$

on $(x,t) \in (0,2) \times (0,1]$, with the following simple smooth initial condition

$$u_0(x) = 0.5 - 0.25\sin(\pi x). \tag{18}$$

The L^1 and L^∞ norms of the numerical errors, and the experimental order of convergence are computed at the final time $t = 1$ in order to avoid the shock formation. All the results are reported in Table 1, Table 2 and Table 3 for different Courant numbers, where we observe third order convergence in both L^1 and L^∞ norms. With large Courant numbers, the proposed two modifications, $\mathsf{Q3P1}_{\mathsf{CEMOOD}}$ and $\mathsf{Q3P1}_{\mathsf{MOOD}}$, reach smaller errors and faster convergence with respect to the results in [4] for the same grid, and the results are similar to those of Q3P1 in [30]. Instead, considering $\Delta t = h$, the conservative a-posteriori time-limiting proposed here performs better than Q3P1 in [30]. This means that the new time-limiting allows to limit less the solution for moderate Courant numbers.
The results related to the proposed $\mathsf{Q3P1}_{\mathsf{MOOD}}$ scheme here reported are obtained with $\alpha_{\mathsf{TL}} = 0.75$. We have not observed changes in the results choosing other values of α_{TL}.

Table 1 Test 1. Comparisons of the orders of convergence of the Quinpi schemes with $\Delta t = h$.

	Q3P1		$\mathsf{Q3P1}_{\mathsf{MOOD}}$		$\mathsf{Q3P1}_{\mathsf{CEMOOD}}$	
N	L^1 error	rate	L^1 error	rate	L^1 error	rate
160	$1.83 \cdot 10^{-3}$	1.71	$7.63 \cdot 10^{-5}$	2.72	$7.63 \cdot 10^{-5}$	2.72
320	$4.27 \cdot 10^{-4}$	2.10	$1.04 \cdot 10^{-5}$	2.87	$1.04 \cdot 10^{-5}$	2.87
640	$7.28 \cdot 10^{-5}$	2.55	$1.34 \cdot 10^{-6}$	2.96	$1.34 \cdot 10^{-6}$	2.96
1,280	$1.00 \cdot 10^{-5}$	2.86	$1.68 \cdot 10^{-7}$	2.99	$1.68 \cdot 10^{-7}$	2.99
2,560	$1.28 \cdot 10^{-6}$	2.97	$2.10 \cdot 10^{-8}$	3.00	$2.10 \cdot 10^{-8}$	3.00

	Q3P1		$\mathsf{Q3P1}_{\mathsf{MOOD}}$		$\mathsf{Q3P1}_{\mathsf{CEMOOD}}$	
N	L^∞ error	rate	L^∞ error	rate	L^∞ error	rate
160	$1.70 \cdot 10^{-2}$	1.09	$8.61 \cdot 10^{-4}$	2.01	$8.61 \cdot 10^{-4}$	2.01
320	$5.51 \cdot 10^{-3}$	1.63	$1.41 \cdot 10^{-4}$	2.61	$1.41 \cdot 10^{-4}$	2.61
640	$1.13 \cdot 10^{-3}$	2.29	$1.88 \cdot 10^{-5}$	2.90	$1.88 \cdot 10^{-5}$	2.90
1,280	$1.64 \cdot 10^{-4}$	2.78	$2.38 \cdot 10^{-6}$	2.98	$2.38 \cdot 10^{-6}$	2.98
2,560	$2.12 \cdot 10^{-5}$	2.95	$2.97 \cdot 10^{-7}$	3.00	$2.97 \cdot 10^{-7}$	3.00

Table 2 Test 1. Comparisons of the orders of convergence of the Quinpi schemes with $\Delta t = 10h$.

	Q3P1		Q3P1$_{\text{MOOD}}$		Q3P1$_{\text{CEMOOD}}$	
N	L^1 error	rate	L^1 error	rate	L^1 error	rate
160	$1.93 \cdot 10^{-3}$	2.05	$1.73 \cdot 10^{-3}$	2.03	$1.72 \cdot 10^{-3}$	1.94
320	$3.75 \cdot 10^{-4}$	2.36	$3.43 \cdot 10^{-4}$	2.34	$3.43 \cdot 10^{-4}$	2.32
640	$6.00 \cdot 10^{-5}$	2.64	$5.57 \cdot 10^{-5}$	2.62	$5.58 \cdot 10^{-5}$	2.62
1,280	$8.25 \cdot 10^{-6}$	2.86	$7.76 \cdot 10^{-6}$	2.84	$7.77 \cdot 10^{-6}$	2.84
2,560	$1.05 \cdot 10^{-6}$	2.97	$1.00 \cdot 10^{-6}$	2.96	$1.00 \cdot 10^{-6}$	2.96
5,120	$1.32 \cdot 10^{-7}$	3.00	$1.26 \cdot 10^{-7}$	2.99	$1.26 \cdot 10^{-7}$	2.99

	Q3P1		Q3P1$_{\text{MOOD}}$		Q3P1$_{\text{CEMOOD}}$	
N	L^∞ error	rate	L^∞ error	rate	L^∞ error	rate
160	$1.59 \cdot 10^{-2}$	1.33	$1.42 \cdot 10^{-2}$	1.26	$1.41 \cdot 10^{-2}$	1.14
320	$4.74 \cdot 10^{-3}$	1.74	$4.33 \cdot 10^{-3}$	1.72	$4.36 \cdot 10^{-3}$	1.69
640	$1.00 \cdot 10^{-3}$	2.24	$9.31 \cdot 10^{-4}$	2.22	$9.33 \cdot 10^{-4}$	2.22
1,280	$1.61 \cdot 10^{-4}$	2.64	$1.52 \cdot 10^{-4}$	2.61	$1.52 \cdot 10^{-4}$	2.61
2,560	$2.18 \cdot 10^{-5}$	2.89	$2.08 \cdot 10^{-5}$	2.87	$2.08 \cdot 10^{-5}$	2.87
5,120	$2.76 \cdot 10^{-6}$	2.98	$2.65 \cdot 10^{-6}$	2.97	$2.65 \cdot 10^{-6}$	2.97

Table 3 Test 1. Comparisons of the orders of convergence of the Quinpi schemes with $\Delta t = 50h$.

	Q3P1		Q3P1$_{\text{MOOD}}$		Q3P1$_{\text{CEMOOD}}$	
N	L^1 error	rate	L^1 error	rate	L^1 error	rate
1,280	$5.67 \cdot 10^{-4}$	2.04	$5.66 \cdot 10^{-4}$	2.03	$5.65 \cdot 10^{-4}$	2.03
2,560	$9.74 \cdot 10^{-5}$	2.54	$9.72 \cdot 10^{-5}$	2.54	$9.73 \cdot 10^{-5}$	2.54
5,120	$1.41 \cdot 10^{-5}$	2.79	$1.41 \cdot 10^{-5}$	2.79	$1.41 \cdot 10^{-5}$	2.79
10,240	$1.90 \cdot 10^{-6}$	2.89	$1.90 \cdot 10^{-6}$	2.89	$1.90 \cdot 10^{-6}$	2.89
20,480	$2.44 \cdot 10^{-7}$	2.96	$2.44 \cdot 10^{-7}$	2.96	$2.44 \cdot 10^{-7}$	2.96

	Q3P1		Q3P1$_{\text{MOOD}}$		Q3P1$_{\text{CEMOOD}}$	
N	L^∞ error	rate	L^∞ error	rate	L^∞ error	rate
1,280	$6.59 \cdot 10^{-3}$	1.48	$6.58 \cdot 10^{-3}$	1.48	$6.54 \cdot 10^{-3}$	1.47
2,560	$1.54 \cdot 10^{-3}$	2.10	$1.54 \cdot 10^{-3}$	2.10	$1.54 \cdot 10^{-3}$	2.09
5,120	$2.69 \cdot 10^{-4}$	2.52	$2.68 \cdot 10^{-4}$	2.52	$2.69 \cdot 10^{-4}$	2.52
10,240	$3.92 \cdot 10^{-5}$	2.78	$3.91 \cdot 10^{-5}$	2.78	$3.91 \cdot 10^{-5}$	2.78
20,480	$5.13 \cdot 10^{-6}$	2.93	$5.13 \cdot 10^{-6}$	2.93	$5.13 \cdot 10^{-6}$	2.93

3.2 Test 2: Linear transport problem

We consider the linear scalar conservation law

$$\partial_t u(x,t) + \partial_x u(x,t) = 0, \tag{19}$$

on $(x,t) \in (-1,1) \times (0,2]$, with periodic boundary conditions in space. As initial condition we will consider the following three profiles:

$$u_0(x) = \sin(\pi x) + \begin{cases} 3, & -0.4 \le x \le 0.4, \\ 0, & \text{otherwise}, \end{cases} \tag{20a}$$

$$u_0(x) = \begin{cases} 1, & -0.25 \le x \le 0.25, \\ 0, & \text{otherwise}, \end{cases} \tag{20b}$$

$$u_0(x) = \begin{cases} \frac{1}{6}\left(G(x,\beta,z-\delta) + G(x,\beta,z+\delta) + 4G(x,\beta,z)\right), & -0.8 \le x \le -0.6, \\ 1, & -0.4 \le x \le -0.2, \\ 1 - |10(x-0.1)|, & 0 \le x \le 0.2, \\ \frac{1}{6}\left(F(x,\alpha,a-\delta) + F(x,\alpha,a+\delta) + 4F(x,\alpha,a)\right), & 0.4 \le x \le 0.6, \\ 0, & \text{otherwise}, \end{cases}$$

where

$$G(x,\beta,z) = \exp(-\beta(x-z)^2),$$
$$F(x,\alpha,a) = \sqrt{\max\{1-\alpha^2(x-a)^2, 0\}}. \tag{20c}$$

The initial conditions (20a) and (20b) are a discontinuous sinusoidal and a double-step profile, respectively, whereas the initial condition (20c) has been designed by Jiang and Shu in [25]. Fixing the constants in (20c) as $a = 0.5$, $z = -0.7$, $\delta = 0.005$, $\alpha = 10$, and $\beta = \log 2/36\delta^2$, this initial condition consists of smooth and non-smooth shapes. Precisely, from the left to the right side of the domain, there is a Gaussian, then a double-step, a sharp triangle and finally a half ellipse.

We use these numerical tests to study the properties of a scheme to transport different shapes with minimal dissipation, dispersion effects and oscillation effects, with different Courant numbers.

Let us focus on the results reported in Fig. 1, obtained using the first initial condition (20a) with two different Courant numbers, i.e. $\mathsf{Cou} = 3$ and $\mathsf{Cou} = 5$. On the left, with $\Delta t = 3h$, we note that the scheme $\mathsf{Q3P1}_{\mathsf{MOOD}}$ with $\alpha_{\mathsf{TL}} = 0$ performs better than the other two implicit schemes. In fact, $\mathsf{Q3P1}_{\mathsf{MOOD}}$ is closer to the exact solution exhibiting lower dissipation. The scheme $\mathsf{Q3P1}_{\mathsf{CEMOOD}}$ is more diffusive but outperforms Q3P1. All the schemes do not oscillate around the discontinuities. Focusing on the right panel of Fig. 1, obtained with a bigger Courant number, $\mathsf{Cou} = 5$, we note that now Q3P1 diffuses less than $\mathsf{Q3P1}_{\mathsf{CEMOOD}}$, but again $\mathsf{Q3P1}_{\mathsf{MOOD}}$, here used with two different values of α_{TL}, provides the best approximation. In particular, choosing $\alpha_{\mathsf{TL}} = 0$ leads to a more dissipative approximation. Instead, a bigger value, $\alpha_{\mathsf{TL}} = 0.75$, which weights less the predictor solution in the time-limiting procedure, allows us to reduce the dissipation error.

In Fig. 2 we observe the results obtained by using the initial condition (20b). We zoom-in the top part of the double-step, in which it is again clear that the $\mathsf{Q3P1}_{\mathsf{MOOD}}$ scheme with $\alpha_{\mathsf{TL}} = 0$ provides the best approximation. In this case, with a smaller Courant number, i.e. $\mathsf{Cou} = 3$, we do not observe oscillations. Instead, with $\mathsf{Cou} = 5$, the $\mathsf{Q3P1}_{\mathsf{MOOD}}$ scheme shows a small undershoot on the bottom part and a small overshoot on the upper part, before the jump discontinuities. Whereas, the

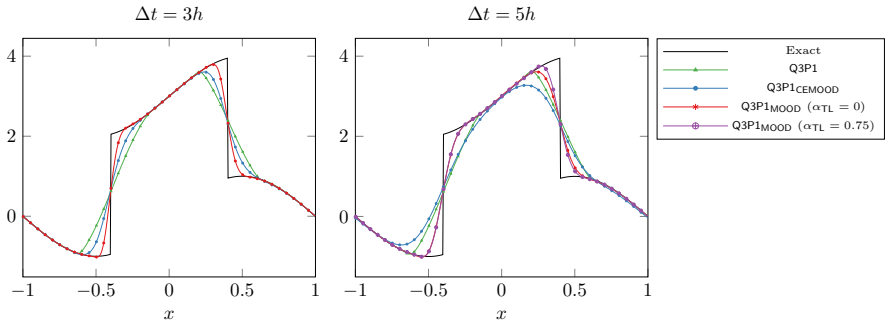

Fig. 1 Test 2. Linear transport equation (19) with initial condition (20a) on 400 cells. The markers are used to distinguish the schemes, and are drawn one out of 10 cells.

Q3P1 scheme shows in addition an undershoot and an overshoot also after the jump discontinuities (see the upper and the bottom parts after the jumps).

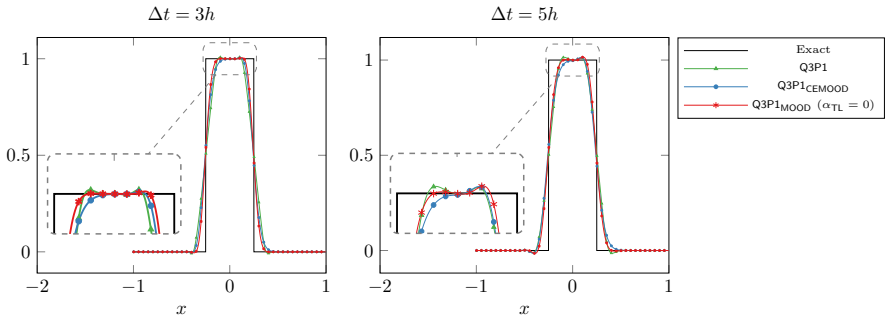

Fig. 2 Test 2. Linear transport equation (19) with initial condition (20b) on 400 cells. The markers are used to distinguish the schemes, and are drawn one out of 10 cells.

We conclude the numerical tests on the linear transport equation with the results reported in Fig. 3, obtained by using the initial condition (20c). Here we use Cou = 2.5 as done in [21]. The scope of this test case is to study the behavior of the scheme Q3P1$_{\text{MOOD}}$ for different values of the parameter that defines the mixing between predictor and corrector. Overall, the best choice is $\alpha_{\text{TL}} = 0.75$. Both $\alpha_{\text{TL}} = 0.75$ and $\alpha_{\text{TL}} = 1$ provide a very high resolution of the half ellipse. On the contrary, the other values are very diffusive. However, the value $\alpha_{\text{TL}} = 1$, which represents the unlimited solution, exhibits several oscillations in the bottom parts of the four shapes and in the upper part related to the square wave.

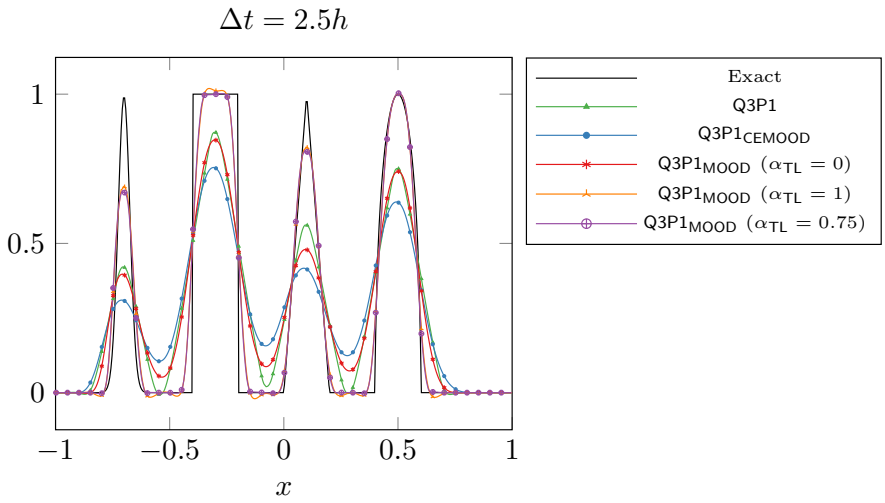

Fig. 3 Test 2. Linear transport equation (19) with initial condition (20c) on 400 cells. The markers are used to distinguish the schemes, and are drawn one out of 10 cells.

3.3 Test 3: Burgers equation

We compare the schemes on the nonlinear Burgers equation (17) studying the following situations.

Test 3a: Shock formation.

We consider again the smooth initial condition (18) on the domain $(x,t) \in (0,2) \times (0,2]$ with periodic boundary conditions in space. The final time is chosen in order to analyze the behavior of the schemes when the shock appears.

In Fig. 4 we show the results obtained with the three third order Quinpi schemes. For a better visualization of the behavior when a shock appears, we have reported the zoom in the bottom left part of the panes obtained with different Courant numbers, i.e. Cou = 3 and Cou = 5. In both cases, we note that the proposed Q3P1$_{\text{MOOD}}$ comes closest to the exact solution on the corners, as clearly visible in the zoom. The other two schemes are more diffusive. Whereas, for Cou = 5 the classical Q3P1 shows a comparable resolution to Q3P1$_{\text{MOOD}}$, and both perform better than Q3P1$_{\text{CEMOOD}}$.

Test 3b: Shock formation and interaction.

Here, we consider the smooth initial condition

$$u_0(x) = 0.2 - \sin(\pi x) + \sin(2\pi x) \tag{21}$$

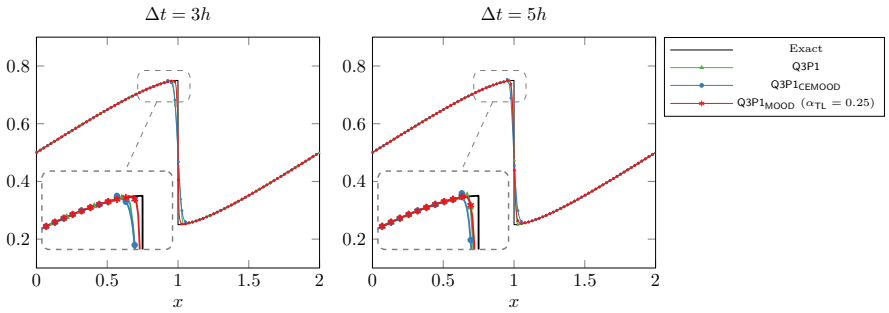

Fig. 4 Test 3a. Burgers equation (17) with initial condition (18) on $N = 400$ cells at time $t = 2$. Cou $= 3$ (on the left), Cou $= 5$ (on the right). The markers are used to distinguish the schemes, and are drawn each 5 cells.

on the space domain $x \in [-1, 1]$ with periodic boundary conditions and fixed Courant number equal to 3, namely $\Delta t = 3h$, studying the behavior of the considered schemes at three different final times. The exact solution is characterized by the formation of two shocks which collide developing a single discontinuity. All the schemes do not produce spurious oscillations at time $t = 1/2\pi$, just before the two shocks appear. Starting from $t = 0.6$, Q3P1$_{\text{CEMOOD}}$ exhibits a small oscillation before the first shock, clearly visible in the zoom part on the left. Moreover, we observe that at time $t = 0.6$ the Q3P1$_{\text{MOOD}}$ scheme is less diffusive than the other two schemes. Similar considerations can be made at time $t = 1$, when the shocks collide.

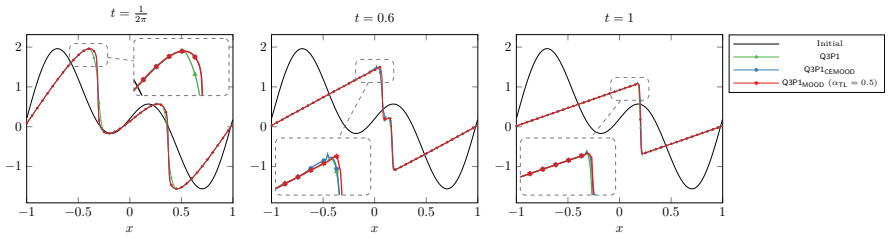

Fig. 5 Test 3b. Burgers equation (17) with initial condition (21) on 400 cells with $\Delta t = 3h$, at three different times. The markers are used to distinguish the schemes, and are drawn each 10 cells.

Test 3c: Rarefaction and shock waves.

Finally, we consider the discontinuous initial condition (20b) on the domain $(x, t) \in (-1, 1) \times (0, 0.5]$, with periodic boundary conditions in space. We reported below the results related to the case with two different Courant numbers.

In Fig. 6, with $\Delta t = 3h$, we observe again that the proposed $\mathsf{Q3P1}_{\mathsf{MOOD}}$ scheme provides the best approximation, followed by the classical Q3P1 proposed in [30], and then by $\mathsf{Q3P1}_{\mathsf{CEMOOD}}$. For the $\mathsf{Q3P1}_{\mathsf{MOOD}}$ scheme, we use the value $\alpha_{\mathsf{TL}} = 0.75$.

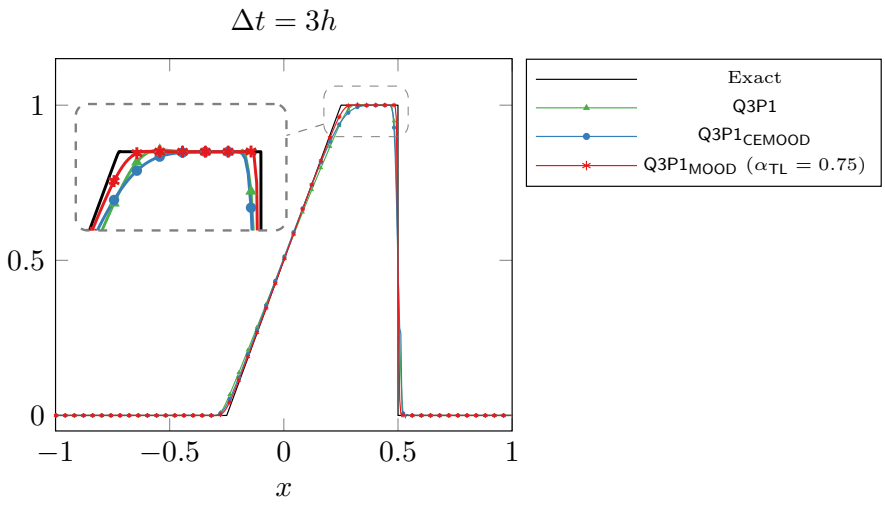

Fig. 6 Test 3c. Burgers equation (17) with initial condition (20b) on 400 cells at time $t = 0.5$, with $\Delta t = 3h$. The markers are used to distinguish the schemes, and are drawn every 8 cells.

Finally, in Fig. 7, obtained with $\Delta t = 5h$, we note that the three schemes are closer to each other in the zoomed part, even if Q3P1 and $\mathsf{Q3P1}_{\mathsf{CEMOOD}}$ perform worse in the bottom part, for example around $x = 0.5$, as expected since with a greater Courant number these schemes diffuse more. We do not observe the same for the $\mathsf{Q3P1}_{\mathsf{MOOD}}$ scheme since we use here the value $\alpha_{\mathsf{TL}} = 0.45$.

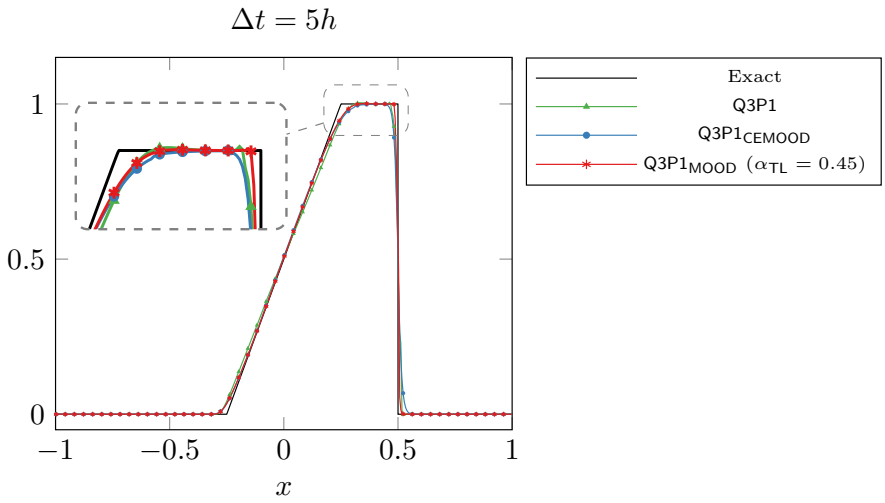

Fig. 7 Test 3c. Burgers equation (17) with initial condition (20b) on 400 cells at time $t = 0.5$, with $\Delta t = 5h$. The markers are used to distinguish the schemes, and are drawn every 8 cells.

3.4 Computational performance of the Quinpi schemes

In the following, we compare the computational CPU times required by each time step of the explicit third order SSP Runge-Kutta scheme and of the Quinpi schemes. In Table 4 we report the results obtained both on the linear equation (19) on $[-1, 1]$ and on the Burgers' equation (17) on $[0, 2]$ with initial condition (18). To make the test reliable and fair, the parameters are chosen to have a comparable and large enough total time of execution of all the methods. The results are obtained on a quad-core Intel Core i7-6600U with clock speed 2.60GHz.

Looking at Table 4, we note that the Q3P1$_{\mathrm{CEMOOD}}$ scheme is the fastest third order scheme in terms of CPU time in all the three problems considered, for all the choices of cells N. Q3P1$_{\mathrm{CEMOOD}}$ is followed by Q3P1$_{\mathrm{MOOD}}$, the slowest one results to be the Q3P1 proposed in [30]. In terms of time ratios, we can note bigger values for Q3P1 scheme, followed by Q3P1$_{\mathrm{MOOD}}$ and then by Q3P1$_{\mathrm{CEMOOD}}$. Of course, the SSP-RK3 explicit scheme is the fastest one, as expected, requiring about a third of the time of the Quinpi schemes in most cases, arriving until more than a quarter of the time of the Quinpi schemes for the last refinement in the nonlinear problem after shock formation.

4 Conclusion and perspectives

Several systems of hyperbolic conservation laws are characterized by waves with very different speeds, and in many applications the phenomenon of interest travels

Table 4 CPU times (in seconds) for each step of the SSP-RK3 explicit scheme, the Q3P1, the $\mathsf{Q3P1}_{\mathsf{MOOD}}$ and the $\mathsf{Q3P1}_{\mathsf{CEMOOD}}$ implicit schemes, on linear and nonlinear problems. The time ratios are given in parenthesis, using as reference the time of the explicit scheme.

Cells N	SSP-RK3	Q3P1	$\mathsf{Q3P1}_{\mathsf{MOOD}}$	$\mathsf{Q3P1}_{\mathsf{CEMOOD}}$
200	0.0021s	0.0062s (2.95)	0.0062s (2.95)	0.0060s (2.86)
400	0.0033s	0.0093s (2.82)	0.0093s (2.82)	0.0082s (2.48)
800	0.0061s	0.0155s (2.54)	0.0151s (2.47)	0.0130s (2.13)
1600	0.0095s	0.0293s (3.08)	0.0272s (2.86)	0.0227s (2.39)

(a) Linear problem.

Cells N	SSP-RK3	Q3P1	$\mathsf{Q3P1}_{\mathsf{MOOD}}$	$\mathsf{Q3P1}_{\mathsf{CEMOOD}}$
200	0.0023s	0.0077s (3.35)	0.0075s (3.26)	0.0068s (2.96)
400	0.0032s	0.0105s (3.28)	0.0105s (3.28)	0.0092s (2.87)
800	0.0066s	0.0182s (2.76)	0.0179s (2.71)	0.0159s (2.41)
1600	0.0091s	0.0344s (3.78)	0.0327s (3.59)	0.0282s (3.10)

(b) Nonlinear problem before shock formation.

Cells N	SSP-RK3	Q3P1	$\mathsf{Q3P1}_{\mathsf{MOOD}}$	$\mathsf{Q3P1}_{\mathsf{CEMOOD}}$
200	0.0023s	0.0099s (4.30)	0.0100s (4.35)	0.0092s (4.00)
400	0.0033s	0.0132s (4.00)	0.0132s (4.00)	0.0115s (3.48)
800	0.0068s	0.0223s (3.28)	0.0220s (3.23)	0.0195s (2.87)
1600	0.0095s	0.0433s (4.56)	0.0418s (4.40)	0.0389s (4.09)

(c) Nonlinear problem after shock formation.

with slow speeds, whereas the fastest waves do not need to be accurately represented. Low Mach problems provide typical examples. In fact, in these cases the actual speed of the gas is much slower than the acoustic waves. However, fast waves impose the Courant-Friedrichs-Levy stability condition, and if one is interested in the movement of the gas, accuracy in the propagation of sound is irrelevant.

These problems require implicit numerical treatment. An implicit third order scheme based on CWENO, named Quinpi, has been recently introduced in [30]. There, the implicit formulation has been tackled using low order linear implicit schemes, the predictor, to avoid the nonlinearities of the high order space reconstruction. In this chapter we have revisited Quinpi schemes by proposing a conservative a-posteriori time-limiting procedure inspired by the MOOD method. The time-limiting blends the low order predictor and the third order solution to dampen possible spurious oscillations due to large time steps. Furthermore, we have built two types of predictors, one based on the composite backward Euler, as in [30], and another one based on the continuous extension of the backward Euler.

We have numerically compared the scheme in [30] with the schemes proposed in this chapter. We have shown that the Quinpi scheme with the conservative a-posteriori time-limiting and with composite backward Euler as predictor performs better than the other two third order Quinpi schemes. In terms of CPU times, the new Quinpi schemes of this work are faster than the classical Quinpi approach in [30]. In particular, the scheme with the predictor based on the continuous extension results to be the fastest one.

Future research will be focused on the extension of the Quinpi approach to systems of conservation laws and on the use of other time integration schemes, such as stage accurate Runge-Kutta and Backward Differentiation Formula solvers.

Acknowledgments

The authors are members of the INdAM Research Group GNCS. This work was partially supported by Ateneo Sapienza project 2019 “Metodi numerici per problemi evolutivi, networks ed applicazioni”, and carried out within the MUR (Ministry of University and Research) PRIN-2017 project “Innovative Numerical Methods for Evolutionary Partial Differential Equations and Applications” (number 2017KKJP4X), Ateneo Sapienza projects 2020 “Algoritmi e modelli per sistemi di natura iperbolica, networks e applicazioni”, and 2021 “Evolutionary problems: analysis techniques and construction of numerical solutions”, INdAM-GNCS project "Metodi numerici per l’imaging: dal 2D al 3D", Code CUP_E55F22000270001.

References

1. Abbate, E., Iollo, A., Puppo, G.: An all-speed relaxation scheme for gases and compressible materials. J. Comput. Phys. **351**, 1–24 (2017)
2. Acker, F., Borges, R.B.d.R., Costa, B.: An improved WENO-Z scheme. J. Comput. Phys. **313**, 726–753 (2016). DOI 10.1016/j.jcp.2016.01.038
3. Alexander, R.: Diagonally implicit Runge-Kutta methods for stiff O.D.E.’s. SIAM J. Numer. Anal. **14**(6), 1006–1021 (1977)
4. Arbogast, T., Huang, C., Zhao, X., King, D.N.: A third order, implicit, finite volume, adaptive Runge-Kutta WENO scheme for advection-diffusion equations. Comput. Methods Appl. Mech. Engrg. **368** (2020). DOI 10.1016/j.cma.2020.113155
5. Avgerinos, S., Bernard, F., Iollo, A., Russo, G.: Linearly implicit all Mach number shock capturing schemes for the Euler equations. J. Comput. Phys. **393**, 278–312 (2019)
6. Boscarino, S., Russo, G., Scandurra, L.: All Mach number second order semi-implicit scheme for the Euler equations of gas dynamics. J. Sci. Comp. **77**(2), 850–884 (2018)
7. Castro, M., Costa, B., Don, W.S.: High order weighted essentially non-oscillatory WENO-Z schemes for hyperbolic conservation laws. J. Comput. Phys. **230**(5), 1766–1792 (2011). DOI 10.1016/j.jcp.2010.11.028
8. Clain, S., Diot, S., Loubère, R.: A high-order finite volume method for hyperbolic systems: Multi-dimensional Optimal Order Detection (MOOD). J. Comput. Phys. **230**(10), 4028–4050 (2011)
9. Clain, S., Diot, S., Loubère, R.: Improved detection criteria for the Multi-dimensional Optimal Order Detection MOOD on unstructured meshes with very high-order polynomials. Comp. & Fluids **64**, 43–63 (2012)
10. Coquel, F., Nguyen, Q.L., Postel, M., Tran, Q.H.: Local time stepping with adaptive time step control for a two-phase fluid system. In: ESAIM: Proceedings, vol. 29, pp. 73–88 (2009)
11. Coquel, F., Nguyen, Q.L., Postel, M., Tran, Q.H.: Entropy-satisfying relaxation method with large time-steps for Euler IBVPs. Math. Comp. **79**, 1493–1533 (2010)
12. Coquel, F., Nguyen, Q.L., Postel, M., Tran, Q.H.: Local time stepping applied to implicit-explicit methods for hyperbolic systems. Multiscale Model. Simul. **8**(2), 540–570 (2010)

13. Coquel, F., Postel, M., Poussineau, N., Tran, Q.H.: Multiresolution technique and explicit–implicit scheme for multicomponent flows. J. Numer. Math. **14**(3), 187–216 (2006)
14. Cravero, I., Puppo, G., Semplice, M., Visconti, G.: CWENO: uniformly accurate reconstructions for balance laws. Math. Comp. **87**(312), 1689–1719 (2018). DOI http://dx.doi.org/10.1090/mcom/3273
15. Cravero, I., Semplice, M., Visconti, G.: Optimal definition of the nonlinear weights in multidimensional Central WENOZ reconstructions. SIAM J. Numer. Anal. **57**(5), 2328–2358 (2019). DOI 10.1007/s10915-015-0123-3
16. Degond, P., Tang, M.: All speed scheme for the low Mach number limit of the isentropic Euler equations. Comm. Computat. Phys. **10**(1), 1–31 (2011)
17. Dellacherie, S.: Analysis of Godunov type schemes applied to the compressible Euler system at low Mach number. J. Comput. Phys. **229**(4), 978–1016 (2010)
18. Dimarco, G., Loubere, R., Vignal, M.H.: Study of a new asymptotic preserving scheme for the Euler system in the low Mach number limit. SIAM J. Sci. Comput. **39**(5), A2099–A2128 (2017)
19. Dimarco, G., Pareschi, L.: Numerical methods for kinetic equations. Acta Numerica **23**, 369–520 (2014). DOI 10.1017/S0962492914000063
20. Duraisamy, K., D. Baeder, J.: Implicit scheme for hyperbolic conservation laws using non oscillatory reconstruction in space and time. SIAM J. Sci. Comput. **29**, 2607–2620 (2007)
21. Eimer, M., Borsche, R., Siedow, N.: Implicit finite volume method with a posteriori limiting for transport networks. Adv. Comput. Math. **48**(3), 21 (2022)
22. Frolkovič, P., Krišková, S., Rohová, M., Žeravý: Semi-implicit methods for advection equations with explicit forms of numerical solution (2022). Preprint arXiv:2106.15474
23. Frolkovič, P., Žeravý: Semi-implicit high resolution numerical scheme for conservation laws (2022). Preprint arXiv:2206.09425
24. Gottlieb, S., Shu, C., Tadmor, E.: Strong stability preserving high-order time discretization methods. SIAM Rev. **43**, 73–85 (2001)
25. Jiang, G.S., Shu, C.W.: Efficient implementation of weighted ENO schemes. J. Comput. Phys. **126**, 202–228 (1996)
26. Lemou, M., Mieussens, L.: A new asymptotic preserving scheme based on micro–macro formulation for linear kinetic equations in the diffusion limit. SIAM J. Sci. Comput. **31**, 334–368 (2008)
27. Levy, D., Puppo, G., Russo, G.: Compact central WENO schemes for multidimensional conservation laws. SIAM J. Sci. Comput. **22**(2), 656–672 (2000). DOI 10.1137/S1064827599359461
28. Loubère, R., Dumbser, M., Diot, S.: A new family of high order unstructured mood and ADER finite volume schemes for multidimensional systems of hyperbolic conservation laws. Comm. Computat. Phys. **16**, 718–763 (2014)
29. Pieraccini, S., Puppo, G.: Microscopically implicit–macroscopically explicit schemes for the BGK equation. J. Comput. Phys. **231**, 299–327 (2012)
30. Puppo, G., Semplice, M., Visconti, G.: Quinpi: Integrating conservation laws with CWENO implicit methods. Comm. Appl. Math. & Comput. (2022). DOI 10.1007/s42967-021-00171-0
31. Semplice, M., Loubère, R.: Adaptive-Mesh-Refinement for hyperbolic systems of conservation laws based on a posteriori stabilized high order polynomial reconstructions. J. Comput. Phys. **354**, 86–110 (2018)
32. Shu, C.W.: Essentially Non-Oscillatory and Weighted Essentially Non-Oscillatory Schemes for Hyperbolic Conservation Laws. NASA/CR-97-206253 ICASE Report No.97-65 (1997)
33. Tavelli, M., Dumbser, M.: A pressure-based semi-implicit space-time discontinuous Galerkin method on staggered unstructured meshes for the solution of the compressible Navier-Stokes equations at all Mach numbers. J. Comput. Phys. **341**, 341–376 (2017). DOI 10.1016/j.jcp.2017.03.030
34. Zanotti, O., Dumbser, M., Loubère, R., Diot, S.: A posteriori subcell limiting for discontinuous Galerkin finite element method for hyperbolic system of conservation laws. J. Comput. Phys. **278**, 47–75 (2014)
35. Zennaro, M.: Natural Continuous Extensions of Runge-Kutta Methods. Math. Comp. **46**, 119–133 (1986)